Journal of Electroceramics, 6, 219–232, 2001

Charge Compensation Mechanisms in La-Doped $BaTiO_3$

FINLAY D. MORRISON,[1] ALISON M. COATS,[2] DEREK C. SINCLAIR[1] & ANTHONY R. WEST[1]

[1]*Department of Engineering Materials, University of Sheffield, Sheffield, S1 3JD, UK*

[2]*Department of Chemistry, University of Aberdeen, Aberdeen AB24 3UE, UK*

Submitted May 25, 2000; Revised February 9, 2001; Accepted March 7, 2001

Abstract. The mechanism of doping $BaTiO_3$ with La has been investigated by a combination of X-ray diffraction, electron probe microanalysis, scanning and transmission electron microscopy and impedance measurements. Phase diagram results confirm that the principal doping mechanism involves ionic compensation through the creation of titanium vacancies. All samples heated in oxygen at 1350–1400°C are electrical insulators, consistent with an ionic compensation mechanism. Samples heated in air or atmospheres of low oxygen partial pressure, at similar temperatures, lose a small amount of oxygen and this gives rise to a second, electronic compensation mechanism in addition to the main, ionic compensation mechanism; as a result, samples are dark-coloured and semiconducting. The change from insulating to semiconducting behaviour is reversible, by changing the atmosphere on heating at 1350–1400°C. We find no evidence for any changes in cationic composition of the $BaTiO_3$ solid solutions arising from changes in oxygen content.

Keywords: doping mechanisms, defects, phase equilibria, conductivity, impedance spectroscopy

Introduction

The defect chemistry of undoped and doped $BaTiO_3$ has been widely studied [1–4]; however, many discrepancies exist between experimental observations and theoretical discussion, especially for La-doped $BaTiO_3$. When La^{3+} replaces Ba^{2+} on the A-site (La is too large to replace Ti on the B-site), charge imbalance is created which must be compensated by either cation vacancies on the A- or B-site (ionic compensation), or by electrons (electronic compensation). Three simple possible mechanisms can be identified:

$$4Ba^{2+} + Ti^{4+} \Rightarrow 4La^{3+} + V_{Ti} \quad (1)$$

$$3Ba^{2+} \Rightarrow 2La^{3+} + V_{Ba} \quad (2)$$

$$Ba^{2+} \Rightarrow La^{3+} + e^{-} \quad (3)$$

These may be written in Kroger–Vink notation as:

$$4Ba_{Ba}^{x} + Ti_{Ti}^{x} \Rightarrow 4La_{Ba}^{\bullet} + V_{Ti}'''' \quad (1')$$

$$3Ba_{Ba}^{x} \Rightarrow 2La_{Ba}^{\bullet} + V_{Ba}'' \quad (2')$$

$$Ba_{Ba}^{x} \Rightarrow La_{Ba}^{\bullet} + e' \quad (3')$$

or in terms of defect reactions as:

$$2La_2O_3 + 3TiO_2 \Rightarrow 4La_{Ba}^{\bullet} + 3Ti_{Ti}^{x} + 12O_O^{x} + V_{Ti}'''' \quad (1'')$$

$$La_2O_3 + 3TiO_2 \Rightarrow 2La_{Ba}^{\bullet} + 3Ti_{Ti}^{x} + 9O_O^{x} + V_{Ba}'' \quad (2'')$$

$$La_2O_3 + 2TiO_2 \Rightarrow 2La_{Ba}^{\bullet} + 2Ti_{Ti}^{x} + 6O_O^{x} + \tfrac{1}{2}O_2 + 2e' \quad (3'')$$

For the latter, if the electrons are associated primarily with Ti, this reaction may be rewritten as:

$$La_2O_3 + 2TiO_2 \Rightarrow 2La_{Ba}^{\bullet} + 2Ti_{Ti}' + 6O_O^{x} + \tfrac{1}{2}O_2$$

Ionic compensation (1, 2) should have negligible effect on the room temperature conductivity due to the immobility of cation vacancies; La-doped $BaTiO_3$ compensated in this way should, therefore, remain insulating. In contrast, electronic compensation (3) should cause a substantial increase in conductivity, in which the number of carriers equals the La concentration. Several studies have used "equilibrium" conductivity measurements as a function of oxygen partial pressure, P_{O_2}, and temperature to determine

the defect chemistry and compensation mechanisms in La-doped $BaTiO_3$, particularly for low La concentrations (<1 at%). The data of Daniels et al. [4] at 1200°C suggest that at low P_{O_2} ($<10^{-7}$ atm) La is electronically compensated, while at higher P_{O_2}, ionic compensation occurs. It was assumed that titanium vacancies would be energetically unfavourable and barium vacancies were therefore assumed to be responsible for ionic compensation. The resulting defect model predicts that, with increasing temperature, the system tends towards electronic compensation even in oxidising (high P_{O_2}) atmospheres such as air. In a similar study, by contrast, the data of Chan et al. indicated that the conductivity in lightly donor-doped $BaTiO_3$ was independent of P_{O_2} [3]. This led to the development of an alternative model (in conflict with that of Daniels et al. [4]), where electronic compensation occurs at all P_{O_2} for donor concentrations of <1 at%.

An alternative approach to obtain information on defect and doping mechanism(s) in La-doped $BaTiO_3$ is to determine the locii of solid solutions in equilibrium phase diagrams and, where possible, link these to crystallographic studies. The three different compensation mechanisms can, in principle, give rise to solid solutions with formulae, $Ba_{1-x}La_xTi_{1-x/4}O_3$ (1‴), $Ba_{1-3y/2}La_yTiO_3$ (2‴) and $Ba_{1-z}La_ze_zTiO_3$ (3‴); these can be distinguished by their loci on the phase diagram Ba-La-Ti-O. Several studies [5–8] have shown the existence of a solid solution of formula (1‴) where $0 \leq x \leq 0.25$ in La doped compositions heated in air at >1300°C. These results are in agreement with the lattice energy calculations of Lewis and Catlow [9] which show that Ti vacancy formation is favoured under these conditions.

The phase diagram results, however, do not correlate with the electrical behaviour of La-doped $BaTiO_3$ ceramics prepared in air at high temperatures, especially for La ≤ 0.5 at%, where samples are dark-coloured and semiconducting at room temperature, Fig. 1. A resistance minimum is observed with increasing La content, and also with other rare earth dopants, including Y, Sm, Gd, Ho and Nd [1, 10–12]. This behaviour is poorly understood, but is usually explained as a switch in compensation mechanism [3, 4, 13, 14], from electronic compensation at low dopant concentrations where the rare earth ion supposedly acts as a donor-dopant,[1] resulting in the resistance drop, to an ionic compensation mechanism at higher concentrations, causing an increase in resistance. This resistance anomaly is only observed in coarse-grained samples which have been

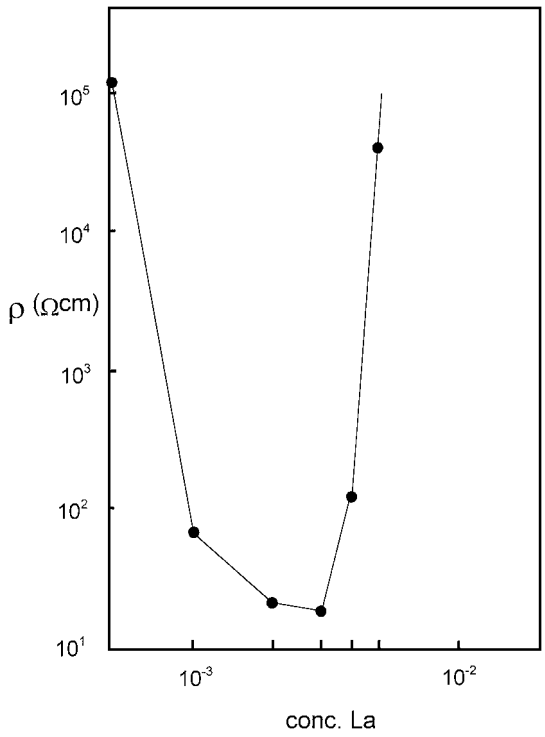

Fig. 1. Resistivity as a function of La concentration for La-doped $BaTiO_3$ [25].

rapidly cooled from high temperatures (≥1350°C) in air, and is therefore attributed to the existence of a non-equilibrium state. Samples which have been slow cooled or annealed at lower temperatures exhibit increased resistances. This observation cannot be explained by the defect model of Chan et al. [3], which predicts electronic compensation and semiconductivity under all conditions. The model of Daniels et al. [4] attributes the dependence on cooling rate to a switch from electronic to ionic compensation mechanisms. Implicit to this change in mechanism is a switch in solid solution formula and hence in both stoichiometry and defect structure. The driving force for such a switch in mechanism remains unclear.

Semiconductivity can be induced in $BaTiO_3$-based materials by a related mechanism, which involves heating pre-reacted samples in a reducing atmosphere [10, 15]; a small amount of oxygen is lost from the crystal lattices of both undoped and doped $BaTiO_3$ leading to n-type semiconductivity:

$$2O^{2-} \Rightarrow O_2 + 4e^- \quad (4)$$

$$O_O^x \Rightarrow \tfrac{1}{2}O_2 + V_O^{\bullet\bullet} + 2e' \quad (4')$$

The defect models of both Chan et al. and Daniels et al. [3, 4] incorporate the suggestion that the extent of reaction (4, 4′) increases with increasing temperature and decreasing P_{O_2} in both undoped and donor-doped $BaTiO_3$. The amount of oxygen loss is small, $\ll 1\%$, and difficult to quantify by thermogravimetric techniques, but nevertheless has a significant influence on the level of electronic conductivity.

Implicit in much of the literature is that, while oxygen loss can certainly occur, Eq. (4), the mechanism based on Eq. (3), is primarily responsible for semiconductivity in La-doped $BaTiO_3$. As far are we are aware, no studies to assess the relative importance of mechanisms (3) and (4) have been made. One of the main problems in studying this is that low La concentrations are involved, typically $\ll 1$ at%. Consequently, the difference in stoichiometry between the various compensation mechanisms is very small, and the presence of any secondary phase associated with a change in mechanism is beyond the detection limits of conventional techniques, such as X-ray diffraction.

The aims of the present study have been to resolve the discrepancies between phase diagram data and reported electrical properties by paying careful attention to sample stoichiometry and to establish which of mechanisms (3) and (4) is primarily responsible for semiconductivity in air-heated samples. This involved accurate determination of phase compositions in reacted samples and measurement of their electrical properties after reaction under different atmospheres. Phase analysis used a combination of X-ray diffraction (XRD), scanning and transmission electron microscopy (SEM, TEM) and electron probe micro analysis (EPMA). Impedance spectroscopy was used to measure electrical properties and assess the relative importance of ionic and electronic compensation mechanisms.

Phase Diagram Considerations

Provided samples remain fully oxidised during synthesis and subsequent heat treatment, and therefore, solid solutions form by either of mechanisms (1) and (2), it is possible to represent La-doped $BaTiO_3$ on the ternary composition triangle $BaO\text{-}La_2O_3\text{-}TiO_2$. In the generation of donor electrons involving mechanisms (3) or (4), some reduction of the Ti^{4+} occurs. These donor electrons must be associated with Ti since Ba and La cannot usually exist in oxidation states less than +II and +III, respectively. Hence, it is necessary to refer such compositions to a partially reduced composition triangle, $BaO\text{-}La_2O_3\text{-}TiO_{1.5}$. The location of these two ternary sections within the quaternary system Ba-La-Ti-O is shown in Fig. 2. These sections have the same cationic compositions irrespective of whether the Ti-based component is TiO_2 or $TiO_{1.5}$. We may, therefore, represent the cationic compositions on a common pseudoternary section $BaO\text{-}La_2O_3\text{-}TiO_x$ and allow the Ti valency to vary, as appropriate. This is shown in Fig. 3; Ti^{3+}-containing phases are shown in italics.

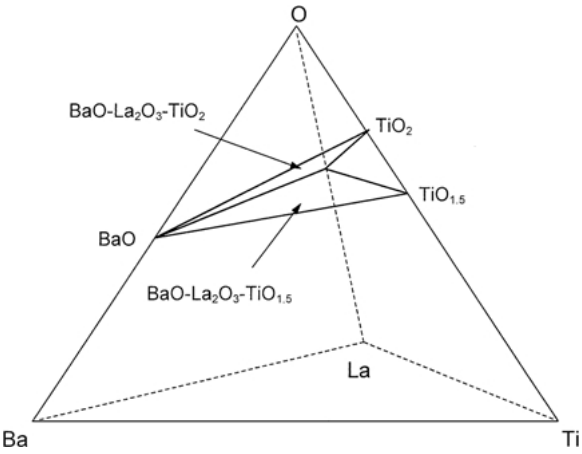

Fig. 2. Composition pyramid Ba-La-Ti-O showing the location of two ternary sections, $BaO\text{-}La_2O_3\text{-}TiO_2$ and $BaO\text{-}La_2O_3\text{-}TiO_{1.5}$.

The three possible mechanisms of charge compensation (1–3), indicated above, are also shown in Fig. 3. The ionic compensation mechanisms leading to either Ti vacancies, (1), or Ba vacancies, (2) are located on the fully oxidised ternary section whereas the electronic compensation mechanism, (3), lies on the partially- reduced section with $LaTiO_3$ as the end-member of the (hypothetical) donor-doped solid solution on complete substitution of Ba by La. Not shown specifically is mechanism (4), simply because this mechanism would have no effect on the cation contents. Hence a combination of (1) and (4) would take the same direction as (1) alone and depending on the degree of oxygen loss, would lie somewhere between the two ternary sections shown in Fig. 2.

This paper is concerned primarily with cationic compositions represented by direction 3 in Fig. 3 since this is the direction taken by the widely-assumed donor- doping mechanism. Depending on whether or not reduction occurs, the reaction products fall into five plausible categories.

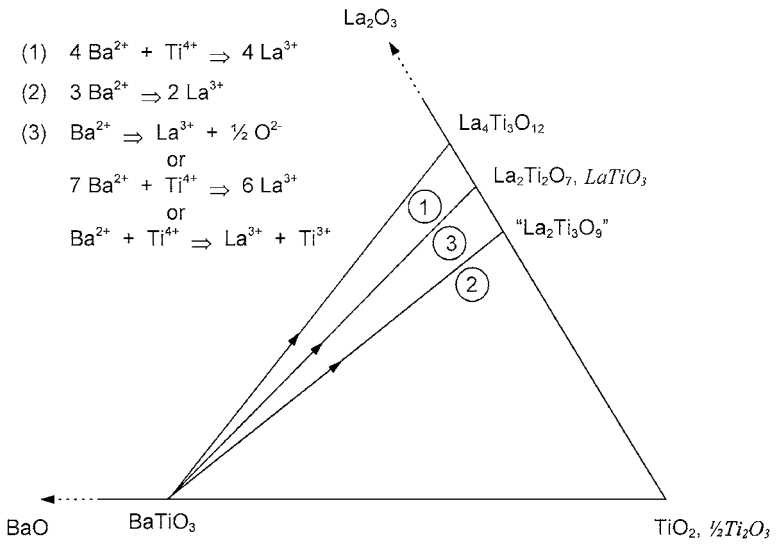

Fig. 3. Compensation mechanisms in La-doped $BaTiO_3$ showing the locus of the possible solid solution directions in the pseudoternary phase diagram BaO-La_2O_3-TiO_x.

(a) Fully oxidised phase mixtures result, consisting of solid solutions on the Ti vacancy join 1, together with other, Ti-rich phase(s).

(b) Fully oxidised phase mixtures result consisting of solid solutions on the Ba vacancy join (2) together with other, Ti-deficient phase(s). There is little evidence for the existence of join 2 in the literature under equilibrium conditions, but it is, at least, theoretically possible.

(c) Fully oxidised single phase solid solutions form in direction 3. This would require one of two possible mechanisms of charge balance, either

(i) creation of interstitial oxide ions by the mechanism

$$Ba^{2+} \Rightarrow La^{3+} + \tfrac{1}{2}O^{2-} \qquad (5)$$

leading to the general formula, $Ba_{1-v}La_v TiO_{3+v/2}$, (the limiting composition of this solid solution, at $v = 1$, is $LaTiO_{3.5}$ ($La_2Ti_2O_7$)), or

(ii) creation of both Ba and Ti vacancies, V_{Ba} and V_{Ti}, by the mechanism

$$7Ba^{2+} + Ti^{4+} \Rightarrow 6La^{3+} + V_{Ba} + V_{Ti} \qquad (6)$$

leading to the general formula, $Ba_{1-w}La_{6w/7}Ti_{1-w/7}O_3$. The limiting composition, at $w = 1$, is also $LaTiO_{3.5}$. Both mechanisms (5) and (6) are plausible, although unlikely.

(d) Fully reduced solid solutions form by the mechanism,

$$Ba^{2+} + Ti^{4+} \Rightarrow La^{3+} + Ti^{3+} \qquad (7)$$

leading to the general formula, $(Ba_{1-y}La_y)(Ti^{4+}_{1-y}Ti^{3+}_y)O_3$. The limiting composition, at $y = 1$, is $LaTiO_3$. Note that (7) is the same as (3) but is specific as to the location of the donated electron.

(e) Solid solutions form with combined ionic and electronic compensation mechanisms, in particular, the combination of the titanium vacancy mechanism (1) and oxygen loss (4). As in the case of (a), additional Ti-rich phase(s) are also needed.

Clearly, the products formed depend on whether or not reduction of Ti^{4+} occurs. If it does, then (d) or (e) are possible; if it does not then one of (a), (b) or (c) should result. The presence of Ti^{3+} should have a significant influence on the level of electronic conductivity. The electrical properties should therefore give a clear indication of any electronic compensation, even for low dopant concentrations, although they cannot distinguish between (d) and (e).

Experimental

Samples were prepared according to mechanisms 1, 2 and 3 with a range of x, y and z values up to ca. 0.30.

Appropriate amounts of $BaCO_3$ (Aldrich, 99.98%), La_2O_3 (Aldrich, 99.99%) and TiO_2 (Aldrich, 99.9+%) were intimately mixed in acetone with an agate mortar and pestle until dry, pressed into pellets using a 13 mm stainless steel die at ∼150 MPa and fired in a Pt crucible in air at 1350°C for 3 days with daily regrinding.

Phase purity was checked by powder XRD using both a Hägg-Guinier camera and a Stoe Stadi P diffractometer. Pellets were analysed using both SEM and EPMA. Back-scattered electron (BSE) images from an ISI SS40 electron microscope were used to detect impurity phases. EPMA used a Cameca SX51 microprobe by measuring L_α lines of Ba and La, and the K_α line of Ti; standards were LaB_6 and benitoite ($BaTiSi_3O_9$). Only cation stoichiometries were analysed; oxygen contents were calculated by difference.

Transmission electron microscopy (TEM) used a JEOL 2000EX TEMSCAN operated at 200 kV. Thin sections were prepared by Ar^+ milling on a Cu grid. Insulating samples were carbon coated to avoid charging under the electron beam. Sample homogeneity across grains and grain boundaries was investigated using energy dispersive x-ray analysis (EDX) via a Link AN 10/85S system.

Pellets for impedance measurements were pressed in an 8 mm stainless steel die at ∼200 MPa and heated on Pt foil in flowing O_2, air or Ar at either 1350 or 1400°C. Pellets fired in air were quenched onto a brass block to reduce surface oxidation during cooling [16]. Samples quenched using this method typically reached room temperature in less than 20–30 seconds. To prepare samples in O_2 and suppress oxygen loss, powders were annealed overnight at 1200°C in flowing O_2, pellets were pressed, sintered at either 1350 or 1400°C and slow-cooled in O_2. All pellets were >95% theoretical density.

All pellets were lightly polished with SiC paper to remove surface roughness and/or surface layers. Semiconducting samples were electroded with InGa alloy (60:40 mole ratio); Au paste (Engelhard T-10112) was applied to insulating samples and hardened by firing in laboratory air at 800°C [7]. The electroded samples were mounted in an impedance jig similar to that described in [17]. In cases where the room temperature resistance was less than ∼1 kΩ, high frequency inductive effects were minimised by using a low inductance jig of similar design to that described in [18]; however, it was not possible to vary temperature using this jig.

Measurements were carried out in laboratory air between 5 Hz and 13 MHz using a Hewlett Packard 4192A Impedance Analyser and between 10^{-2} Hz and 65 kHz using combined 1250/1287 Solartron instrumentation with an applied voltage of 100 mV. Data were corrected for sample geometry and analysed using a combination of in-house software and ZView (Version 1.5) [19].

Impedance Data Analysis

All impedance data were modeled on an equivalent circuit consisting of two parallel resistor-capacitor (RC) elements placed in series, as conventionally used to describe $BaTiO_3$ ceramics [20]. In order to separate the RC elements and determine their component R and C values, analysis using both impedance and electric modulus formalisms was employed [21].

Each RC element gives rise to a semicircle in the complex plane plot (Z'' vs. Z', M'' vs. M') and a Debye peak in the spectroscopic plots of the imaginary component (Z'', M'' vs. f). The origin of a Debye peak is described by the equation for the imaginary components for a parallel RC element [22]:

$$Z'' = R\left[\frac{\omega RC}{1+(\omega RC)^2}\right] \tag{8}$$

$$M'' = \frac{\varepsilon_0}{C}\left[\frac{\omega RC}{1+(\omega RC)^2}\right] \tag{9}$$

where ω is the angular frequency ($2\pi f$) and ε_0 is the permittivity of free space, 8.854×10^{-14} F cm^{-1}. The term in square brackets is the same in Eqs. (8) and (9) and describes the functional form of the Debye peak.

The size of the Debye peaks in the spectroscopic plots scale according to R for Z'' spectra, Eq. (8), and C^{-1} for M'' spectra, Eq. (9). Consequently, impedance spectra and complex plane plots are dominated by those RC elements with the largest R values whereas the M'' spectra and modulus complex plane plots are dominated by those elements with the smallest C values.

Apart from the magnitudes of Z'' and M'', the frequency at which a Debye peak appears can provide important information. The frequencies of peak maxima are given by

$$\omega_{max} = (RC)^{-1} = \tau^{-1} \tag{10}$$

where RC is the time constant, τ, of that particular RC element; τ is an intrinsic property of RC elements since it is independent of geometry.

Our strategy in impedance data analysis was to first make a visual inspection of Z″, M″ spectroscopic plots. This gives information on the number of distinct electrically-active regions present and, from the magnitudes of their capacitances, a first assignment to bulk, grain boundary, surface layer, etc. regions. Reasonably accurate values of the *R* and *C* components are obtained from the intercepts in the complex plane plots, in the usual way. As a final stage in analysis, it is possible to fit the data to more complex circuits containing frequency-dependent admittances and to obtain estimates of departures from ideality implicit in the use of simple RC elements. We have not carried out such fits here due to the large number of data sets involved, the time consuming nature of the fitting and the limited amount of extra information that is obtained, especially regarding the magnitudes of the key *R* and *C* components.

Results

Phase Analysis by XRD, SEM and EPMA

Initially, compositions prepared according to the electronic compensation formula (3‴) were studied. For small z, differences in stoichiometry between this mechanism and other possible mechanisms are very small, Fig. 3. For this reason, high La contents, $z \approx 0.25$, were investigated initially; the La content was subsequently lowered, systematically, to those concentrations ($z \leq 0.01$) commonly used to induce semiconductivity in air-fired, La-doped $BaTiO_3$. Samples were reacted in air at 1350°C; no special steps were taken to avoid oxygen loss. The samples were generally dark grey and, therefore, a significant presence of Ti^{3+} was anticipated.

XRD results showed the presence of two phases for $z = 0.25$, a cubic $BaTiO_3$ pattern and some very faint extra reflections consistent with $Ba_6Ti_{17}O_{40}$ [23]. For lower values of z, all samples appeared to be a single phase $BaTiO_3$ solid solution with varying degrees of tetragonality, depending on the La content. For samples with $z \geq 0.10$, BSE imaging by SEM indicated clearly the presence of two phases, whereas samples with $z \geq 0.20$ contained three phases. For samples with $z < 0.10$, the small volume fraction of any secondary phase made it difficult to differentiate between topological features and intergranular, minor phase(s) in BSE images.

By EPMA, using elemental mapping, small regions of $Ba_6Ti_{17}O_{40}$ were clearly detected in e.g. $z = 0.05$. The lower limit of z at which secondary phases could be detected by EPMA, which has a resolution of ∼1 μm, was ∼0.03. EPMA was also used to determine absolute cation contents in several samples. In addition to samples prepared on line 3, (B1–B5), a range of samples prepared according to the Ba vacancy mechanism, line 2 (samples A1–A4), were analysed, Table 1. All were phase mixtures but the stoichiometry of the main phase in each was consistent with a $BaTiO_3$ solid solution formed by the Ti vacancy mechanism (1). No evidence of compensation according to the Ba vacancy, (2), or electronic (3), mechanisms was observed. For samples y, $z < 0.20$ the minor phase, where detected, was $Ba_6Ti_{17}O_{40}$. The minor phases in samples $z \geq 0.20$ were $Ba_6Ti_{17}O_{40}$ and $Ba_6La_8Ti_{18}O_{54}$, in agreement with the recent study by Škapin et al. [8].

A range of samples on the Ti vacancy join, line 1, was also studied. Those with $x < 0.25$ were phase-pure by XRD, SEM and EPMA. Results on these samples and the variation of properties with composition, including a full characterisation of their electrical properties are reported elsewhere [16, 24].

From the above study, the limits of XRD, SEM and EPMA for detecting the presence of minor phases in this system were determined. Using the phase diagram results and the lever rule, and working on the assumption that the (Ba, La)TiO_3 solid solution exists according to the Ti vacancy mechanism, the amount of $Ba_6Ti_{17}O_{40}$ present in each composition was predicted. Results for samples prepared according to mechanism (3) samples a–f, Table 2 show that the lower detection limit by XRD is ∼5%, by SEM is ∼2% and by EPMA ∼1.5%.

Although the existence of an extensive Ti vacancy solid solution has been reported by several authors [5–8], many studies have claimed that the solid solution formed at low La contents (<1% substitution for Ba) has general formula (3‴) [4, 10–13, 25–28]. At these low levels of La-doping, however, XRD, SEM and even EPMA are insensitive to the small differences in stoichiometry associated with the various solid solution formulae and to the possible presence of secondary phases. The electronic compensation mechanism is generally assumed to hold because of the semiconductivity observed but we question whether there is any direct evidence for the existence of solid solutions on join 3 under the conditions usually used in ceramic fabrication. In addition, most studies do not consider the

Table 1. Comparison of starting compositions for Ba vacancy (A1–4) and electronic (B1–5) compensation solid solutions and observed composition of solid solution (main phase) formed, as determined by EPMA, for samples fired at 1350°C in air. Values given are averaged from 10–20 spot analyses.

	Starting composition (mol%)			Composition of solid solution formed (mol%)			
Sample	BaO	La_2O_3	TiO_x	BaO	La_2O_3	TiO_x	Calculated formula[a]
A1, $y = 0.20$	38.89	5.55	55.56	42.50 ± 0.49	6.21 ± 0.43	51.29 ± 0.22	$Ba_{0.77\pm0.01}La_{0.23\pm0.01}Ti_{0.93\pm0.01}O_3$
A2, $y = 0.15$	41.89	4.06	54.05	43.83 ± 0.32	4.55 ± 0.08	51.62 ± 0.26	$Ba_{0.83\pm0.01}La_{0.17\pm0.01}Ti_{0.97\pm0.01}O_3$
A3, $y = 0.15$	41.89	4.06	54.05	44.12 ± 0.24	4.45 ± 0.16	51.43 ± 0.13	$Ba_{0.83\pm0.01}La_{0.17\pm0.01}Ti_{0.97\pm0.01}O_3$
A4, $y = 0.10$	44.74	2.63	52.63	47.03 ± 0.44	2.48 ± 0.08	50.49 ± 0.28	$Ba_{0.90\pm0.01}La_{0.10\pm0.01}Ti_{0.97\pm0.01}O_3$
B1, $z = 0.25$	40.00	6.67	53.33	41.38 ± 1.50	7.32 ± 1.15	51.30 ± 0.14	$Ba_{0.74\pm0.03}La_{0.26\pm0.02}Ti_{0.92\pm0.01}O_3$
B2, $z = 0.20$	42.11	5.26	52.63	44.00 ± 0.21	4.70 ± 0.13	51.30 ± 0.19	$Ba_{0.82\pm0.01}La_{0.18\pm0.01}$ $Ti_{0.96\pm0.01}O_3$
B3, $z = 0.15$	44.16	3.90	51.95	44.18 ± 0.24	4.32 ± 0.16	51.50 ± 0.13	$Ba_{0.84\pm0.01}La_{0.16\pm0.01}$ $Ti_{0.98\pm0.01}O_3$
B4, $z = 0.10$	46.15	2.57	51.28	46.46 ± 0.18	2.60 ± 0.03	50.94 ± 0.13	$Ba_{0.90\pm0.01}La_{0.10\pm0.01}Ti_{0.98\pm0.01}O_3$
B5, $z = 0.08$	46.94	2.04	51.02	47.21 ± 0.20	2.08 ± 0.02	50.71 ± 0.15	$Ba_{0.92\pm0.01}La_{0.08\pm0.01}Ti_{0.99\pm0.01}O_3$

[a]Analysed compositions fall on Ti vacancy join, 1; the formulae were calculated after normalising Ba + La = 1.

possibility of semiconductivity resulting from oxygen deficiency (4), even for samples heated to high temperatures (>1350°C) in air.

Impedance Measurements

Composition $z = 0.003$ in $Ba_{1-z}La_zTiO_3$. An alternative approach to distinguish between electronic and ionic compensation measurements was to carry out electrical property measurements and to look for the presence or absence of semiconductivity. Samples of $z = 0.003$ in $Ba_{1-z}La_zTiO_3$ were characterised by impedance spectroscopy after heating in both flowing O_2 and laboratory air at 1400°C. This composition is close to that of the resistance minimum for samples heated in air, Fig. 1. The samples were single phase by XRD, SEM and EPMA and exhibited a uniform grain size distribution of 1–2 μm.

A pellet slow-cooled after heating in O_2 at 1400°C was off-white and insulating. The impedance complex plane plot, Z*, at 25°C, Fig. 4(a), showed the high frequency end of a semicircular arc with associated resistance $>10^7\,\Omega$. C was obtained from the effective parallel capacitance and was essentially frequency independent with a value of ~145 pF, consistent with an insulating, bulk response in $BaTiO_3$ [7]. A combined

Table 2. Mole fraction of minor phase present in $Ba_{1-z}La_zTiO_3$ samples (see Fig. 4), as predicted by the lever rule and assuming the Ti vacancy compensation solid solution.

			Second phase detected by		
Sample	Composition (z in $Ba_{1-z}La_zTiO_3$)	Mole fraction $Ba_{0.26}Ti_{0.74}O_{1.74}$ ($\equiv Ba_6Ti_{17}O_{40}$) (mol%)[a]	XRD	SEM	EPMA
a	0.20	5.3	Yes	Yes	Yes
b	0.10	2.5	No	Yes	Yes
c	0.08	2.2	No	No	Yes
d	0.05	1.4	No	No	Yes
e	0.03	0.9	No	No	No
f	0.003	~0.01	No	No	No

[a]The BaO-La_2O_3-TiO_2 ternary phase diagram illustrated the relationship between compounds according to the ratio of constituent oxides. $BaTiO_3$, for example, contains 50 mol% BaO and 50 mol% TiO_2 and is therefore represented by $Ba_{0.5}Ti_{0.5}O_{1.5}$. Similarly, $Ba_6Ti_{17}O_{40}$ contains ca. 26 mol% BaO and 74 mol% TiO_2 and is represented as $Ba_{0.26}$ $Ti_{0.74}O_{1.74}$ (although conventionally the compounds are expressed with whole numbers of atoms, i.e. $BaTiO_3$ and $Ba_6Ti_{17}O_{40}$). The lever rule calculation therefore gives the amount of $Ba_6Ti_{17}O_{40}$ expressed as a mole fraction of $Ba_{0.26}Ti_{0.74}O_{1.74}$.

Z″, M″ spectroscopic plot, Fig. 4(b), showed that the Z″, M″ data were dominated by the low frequency response which indicated a high resistance, low capacitance parallel RC element again consistent with an insulating, bulk response [20]. At higher frequencies ($>10^3$ Hz), the M″ data start to rise slowly. This phenomenon is also observed in undoped $BaTiO_3$ and may result from either stray capacitance and/or inductance effects associated with the conductivity jig or ac losses associated with the ferroelectric domains.

Impedance data obtained at $T > 300$°C (not shown) indicated Debye-like peaks in both Z″ and M″ data. The frequency of the M″ peak was one order of magnitude higher than that of the Z″ peak. From the magnitude of

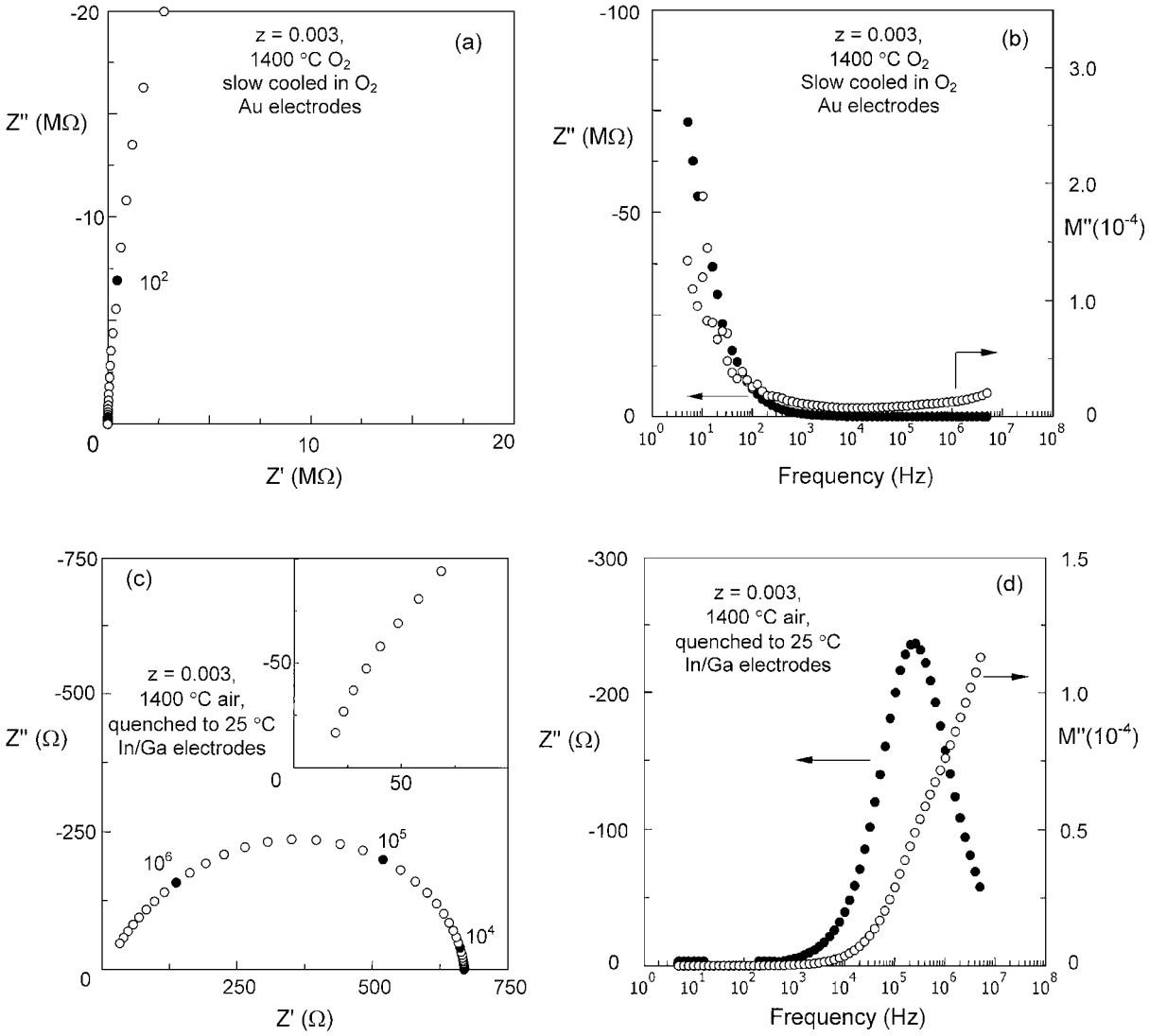

Fig. 4. Room temperature Z*, (a), and combined Z″, M″ spectroscopic plots, (b), for $z = 0.003$ in $Ba_{1-z}La_zTiO_3$ heated at 1400°C in O_2. Room temperature Z*, (c), and combined Z″, M″ spectroscopic plots, (d), for $z = 0.003$ heat treated in air at 1400°C. M″ spectroscopic plots, (e), comparing room temperature data for $z = 0.003$ heat treated at 1400°C in air (●) and O_2 (■). Also shown are data for undoped $BaTiO_3$ also fired at 1400°C in O_2 (◆). Room temperature Z*, (f), and combined Z″, M″ spectroscopic plots (g) for $z = 0.003$ heated treated in O_2 followed by 30 mins in air, both at 1400°C. Filled circles in Z* plots represent selected frequencies in Hz.

(*Continued on next page*.)

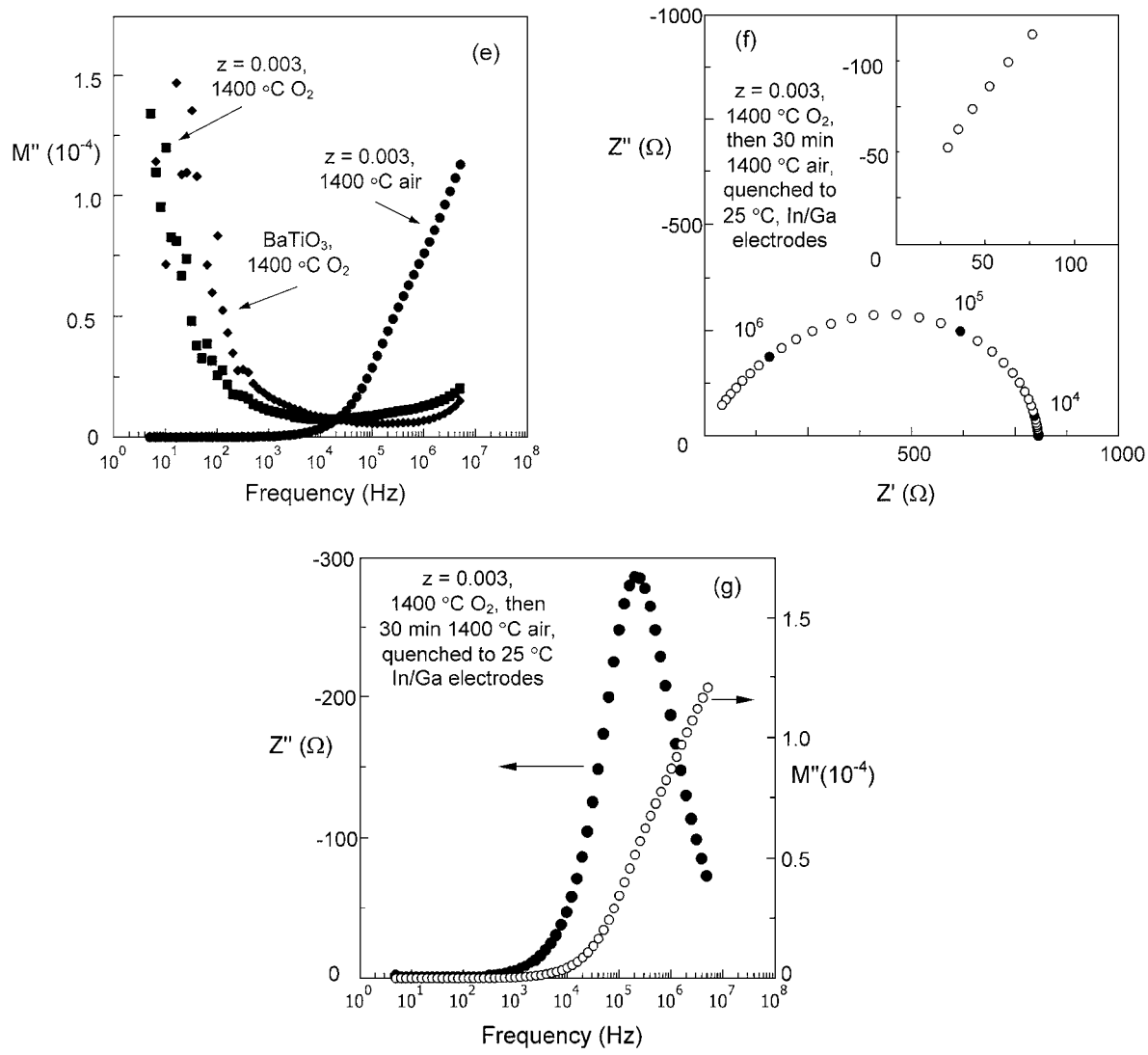

Fig. 4. (*Continued*).

the capacitances (0.3 nF, Z″ and 36.8 pF, M″ at 488°C), the responses were attributed to grain boundary and bulk components [24].

A second pellet of the same composition was fired in air at 1400°C, and quenched to room temperature on a brass block. The pellet was dark grey and its impedance response differed greatly from that of the sample heated in O_2. The Z* plot at 25°C consisted of a single arc with a non-zero intercept on the real axis, Fig. 4(c) with $R \sim 675\ \Omega$ and $C \sim 0.9$ nF, which was attributed to grain boundary regions. The high frequency, non-zero intercept, indicated the presence of another, low resistance region which was confirmed by the Z″, M″ spectroscopic plots, Fig. 4(d): the M″ data, show the start of a second, high frequency ($>10^5$ Hz) peak with a shoulder on the low frequency side coincident with the Z″ peak. The high frequency response which dominates the M″ data is attributed to the bulk (grain interior) response. No maximum is present for the high frequency M″ peak but an associated resistance of $\sim 15\ \Omega$ was estimated from the high frequency intercept on the Z* plot, Fig. 4(c).

Figure 4(e) compares room temperature M″ data for the above two samples with that of undoped

$BaTiO_3$ sintered at 1400°C and slow cooled in O_2. M″ data for the samples heated in O_2 are very similar and indicate the bulk response at low frequencies with a high associated resistance. This suggests that both bulk and grain boundary regions are insulating and that no semiconductive grain interior is present, in contrast to the sample heated in air.

The sample of $z = 0.003$ heated in O_2 was reheated in air at 1400°C for 30 min and air-quenched. Its colour changed from off-white to dark grey. Its impedance response (not shown) was very similar to that of the original sample heated in air, Figs. 4(c) and (d), with a semicircular arc in the Z* plot attributed to the grain boundary response ($R \sim 810\ \Omega$, $C \sim 0.8$ nF) and a high frequency intercept of ∼12 Ω. The Z″, M″ spectroscopic plot was very similar to (d), again confirming the presence of a low R, low C response corresponding to a semiconducting bulk and a somewhat more resistive grain boundary.

The electrical properties of these samples are clearly very sensitive to oxygen content and to subsequent oxygen loss from previously-reacted samples. Pellets heated in O_2 were insulating and, therefore, electronic compensation via mechanism (3), did not occur. This, together with the EPMA results, clearly shows that the primary compensation mechanism is via creation of Ti vacancies (1) and that there is no additional, secondary electronic compensation. By contrast, samples heated in air demonstrate that oxygen vacancies are created at high temperatures and are the source of the semiconductivity under these conditions. Compositions prepared according to the donor-doping mechanism (3), therefore, form multiphase samples according to category (a) when heated in O_2, and category (e) when heated in air.

Composition $x = 0.03$ in $Ba_{1-x}La_xTi_{1-x/4}O_3$. From the above observations on $z = 0.003$, it should be possible to prepare single phase materials based on the titanium vacancy mechanism (1) which also have a range of electrical properties that depend on sample history. In order to test this, a heavily-doped composition with $x = 0.03$, mechanism (1), was studied. When heated to 1350°C in O_2, it was white and had a room temperature impedance response similar to that in Fig. 4(a, b). The sample was insulating, with no sign of any semiconducting regions. At high temperatures (>ca. 300°C), impedance data indicated two Debye-like peaks, one dominated M″ and the other Z″, consistent with insulating bulk and grain boundary responses, respectively [24].

A second pellet of composition $x = 0.03$ was grey after heating to 1350°C in air followed by quenching. Impedance spectroscopy showed the pellet to be electrically inhomogeneous, with several regions of varying resistance. These variations in R were attributed to regions with varying degrees of oxygen loss. Characterisation of such inhomogeneous samples are discussed elsewhere [16].

A third pellet of the same composition was dark grey after heating to 1350°C in Ar and slow cooled to room temperature in Ar. Room temperature impedance data showed a single arc ($R \approx 520\ \Omega$, $C \approx 1.9$ nF) associated with the grain boundary response, and a high frequency, non-zero intercept of ∼12 Ω, Fig. 5(a), associated with the bulk response; M″ data were dominated by the low R, low C response at high frequency, Fig. 5(b), confirming the presence of a semiconducting bulk component.

All three samples exhibited similar ceramic microstructure with a uniform grain size of 2–3 μm.

TEM Analysis

The above experiments showed that a sample on the titanium vacancy join (1) could be either insulating when fully oxidized or semiconducting after a small amount of oxygen loss. In order to determine whether any additional changes occurred, such as a switch in doping mechanism from Ti vacancy (1) to electronic compensation (3), TEM analysis was carried out on samples $x = 0.03$ heated in O_2 and Ar. Although only very small regions of each were analysed, EDX analysis across individual grain boundaries, triple point junctions and within grains showed no evidence of segregation or precipitation of secondary phases in either sample. This indicates that no change in solid solution mechanism occurs, in contrast to the results of Chan and Smyth on Nb-doped $BaTiO_3$ [29]. The different heat treatments therefore yielded samples that were single phase solid solutions, with the same overall cation stoichiometry, but with major differences in electrical properties attributable entirely to their oxygen contents. These results suggest that a switch from the Ti-vacancy, (1), to electronic compensation mechanism, (3), is improbable in samples heated in air or argon and that, instead, the semiconductivity is associated entirely with the creation of oxygen vacancies.

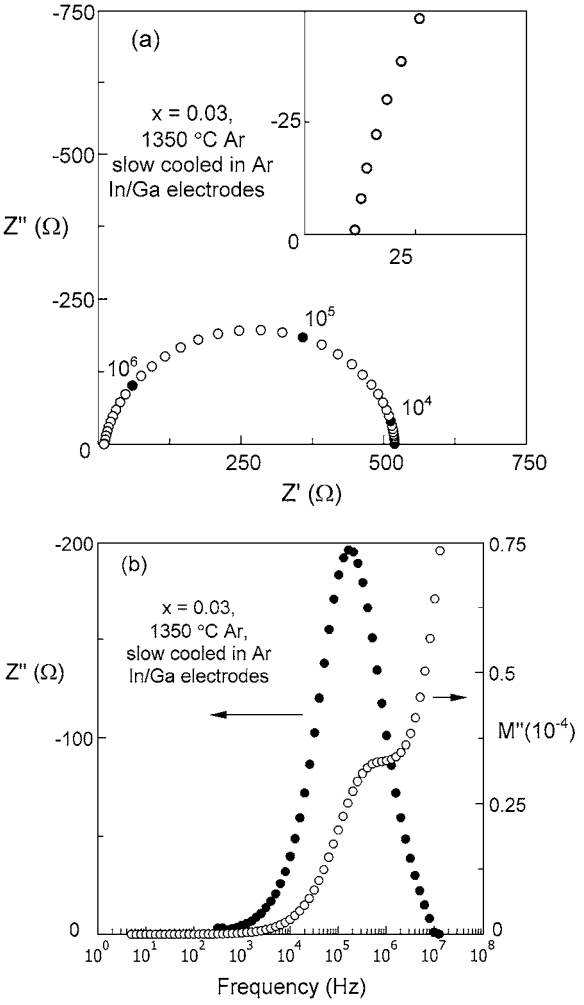

Fig. 5. Room temperature Z*, (a) plot and combined Z″, M″ spectroscopic plot, (b), for $x = 0.03$ in $Ba_{1-x}La_xTi_{1-x/4}TiO_3$ heated at 1350°C in Ar. Filled circles in Z* plot represent selected frequencies in Hz.

Discussion

Several problems exist pertaining to the defect models derived from equilibrium conductivity measurements as a function of P_{O_2} and temperature. Firstly, the electrical measurements were typically carried out using *dc* techniques and provide data only on the total sample resistance without any information on the electrical microstructure and homogeneity of ceramics. Using impedance spectroscopy, we have recently shown that La-doped $BaTiO_3$ compositions may be electrically heterogeneous when heated in air. Such samples exhibit regions of varying resistance including semiconducting grain centres and insulating grain or ceramic surfaces [16].

The defect model of Chan et al. [3] is largely based on their observation that: "$BaTiO_3$ doped with small amounts of donor impurities (<0.5 at%) on either the A or B site is dark-coloured and semiconducting, independent of both the oxygen partial pressure with which it was equilibrated and the A/B ratio". This statement is not supported by our results. If prepared under conditions of low P_{O_2}, La-doped $BaTiO_3$ is dark coloured and semiconducting. In air at e.g. 1350°C, and especially after slow cooling samples, may be partially oxidized with insulating surface layers and semiconducting cores [16], whereas samples heated at 1350°C in flowing O_2 are fully oxidized [24].

For the model of Daniels et al., the hypothesis that a switch from electronic to ionic compensation occurs with decreasing temperature at high P_{O_2}, e.g. in air, is based entirely on chemical diffusivity, $\tilde{D}$, data calculated from conductivity equilibration times under oxidising conditions [4]. For undoped $BaTiO_3$, the chemical diffusivity, $\tilde{D}$, was of the order 10^{-5} cm^2 s^{-1} at 1000°C and obeyed flat plate boundary conditions. Under these conditions, $\tilde{D}$ was attributed to exchange of oxygen with the gas ambient and diffusion throughout the ceramic. On La-doping, $\tilde{D}$ was significantly lower, of the order of 10^{-12} cm^2 s^{-1} at 1000°C, and obeyed spherical boundary conditions. Daniels et al. assumed that, as no change in the oxygen sublattice should occur on La-doping, no change in oxygen diffusivity should be observed. As a result, the low chemical diffusivity was attributed not to oxygen diffusion but to that of barium vacancies [4].

Given that the diffusion of oxygen through a perovskite lattice is most likely to occur via vacant site hopping, the oxygen diffusivity will depend largely on the presence of a significant concentration of oxygen vacancies, $[V_O^{\bullet\bullet}]$. In undoped $BaTiO_3$ the presence of extrinsic acceptor impurities and intrinsic Schottky disorder results in the presence of a small number of oxygen vacancies [1, 2, 4], even under oxidising conditions. On La-doping, these oxide vacancies are extinguished as charge compensation for La^{3+} viz.

$$La_2O_3 + V_O^{\bullet\bullet} \Rightarrow 2La_{Ba}^{\bullet} + 3O_O^x \qquad (11)$$

This is consistent with the displacement of conductivity-P_{O_2} curves to higher P_{O_2} values on donor doping. Under conditions where $[V_O^{\bullet\bullet}]$ is negligible e.g. in

donor-doped $BaTiO_3$ at high P_{O_2}, the oxygen diffusivity is determined by the oxygen self diffusion rate, i.e. the diffusion rate in the absence of a significant P_{O_2} gradient [30].

Shirasaki et al. measured the self-diffusion coefficient of oxygen, D_O, in La-doped $BaTiO_3$ ceramics using O^{18} tracer measurements and determined that $D_O \approx 10^{-13}$ at 1000°C [31], similar to the $\tilde{D}$ value determined by Daniels et al. [4].

In undoped and donor doped $BaTiO_3$ ceramics at low P_{O_2}, the concentration of $V_O^{\bullet\bullet}$ in the bulk means that the bulk oxygen diffusion coefficient, D_b is similar to that of the grain boundary, D_{gb}. Oxygen diffusion and equilibration with the gas ambient is therefore rapid and homogeneous from the ceramic surface throughout the sample obeying flat plate boundary conditions of diffusion. In donor doped $BaTiO_3$ at high P_{O_2}, where $[V_O^{\bullet\bullet}]$ is negligible, D_b is $\ll D_{gb}$. Equilibration of the grain centres (bulk) with the P_{O_2} atmosphere is now rate determining. In this case, diffusion obeys the spherical boundary conditions determined by the grain morphology. On rapid cooling, therefore, oxygen-deficient, semiconducting grains result. Under the appropriate conditions, sufficient grain boundary reoxidation occurs to result in a PTCR effect [27, 28].

This scenario is consistent both with the observed decrease in $\tilde{D}$ and the change in boundary conditions of the diffusion behaviour on La-doping. This explanation is also consistent with the formation of insulating surface layers observed in air-heated La-$BaTiO_3$ ceramics [16, 32]. This scenario of diffusion behaviour and the resulting effect on the extent and distribution of re-oxidation in transition metal perovskites has been shown experimentally and theoretically by Maier et al. [33–35].

The proposal that semiconductivity results directly from oxygen deficiency correlates well with several other observations in the literature. The room temperature resistance of La-doped samples heated in air was highly dependent on a number of variables, including composition, grain size, pellet density and sample history [36]. Samples prepared in air at $T < 1350$°C, were insulating whereas, those prepared at $T > 1350$°C were semiconducting [37]. Equilibrium conductivity studies on undoped and donor-doped $BaTiO_3$ showed that the number of oxygen vacancies, and therefore conductivity, increased with both increasing temperature and decreasing P_{O_2} [2–4]. In order to observe semiconductivity, it is important to quench samples in order to "freeze in" oxygen vacancies created at high temperature; slow cooled samples exhibit much higher resistances [12, 38] because reoxidation results in "back-filling" of the vacancies created at high temperatures. MacChesney et al. [39] suggested that "bodies exhibiting semiconductivity do not achieve equilibrium during air firing"; instead a metastable semiconducting state may exist as semiconductivity is observed only in samples which have been "fired rapidly at temperatures within a restricted range". They noted that heating and cooling rates, temperature and heating duration were important factors in determining the level of resistivity of La-doped $BaTiO_3$ compositions.

The resistivity minimum observed on doping $BaTiO_3$ with La, Fig. 1, is widely attributed to a change in doping mechanism, from one of electronic compensation to one of ionic compensation with increasing La content. It is now well-established, from this and other work, that the prime doping mechanism in air-heated ceramics involves ionic compensation (1–1‴) at all La contents. Any switch in mechanism from electronic (3–3‴) to ionic (1–1‴) would necessarily involve a change in cation stoichiometry, from line (3) to line (1) in Fig. 3, together with precipitation of a Ti-rich phase. Conversely, a switch from (1‴) to (3‴) would necessitate precipitation of a Ba-rich phase.

The traditional view of defect equilibria in doped $BaTiO_3$ is based on reactions such as (1″) to (3″); for (3″) in particular, the oxygen content is adjusted, by release of O_2 gas, to give rise to an effective electronic compensation mechanism. We prefer an alternative approach which makes no assumptions about the effects, if any, on cation stoichiometry in air-heated ceramics. This approach has two components.

First, for samples heated under suitably oxidising conditions, a purely ionic mechanism of charge compensation for La^{3+}-doping occurs, (1–1‴). Second, for such samples heated in atmospheres of low P_{O_2}, an additional mechanism involving loss of oxygen from the crystal lattice and associated electronic compensation (4, 4′) occurs. This mechanism does not modify the cationic composition and in particular, does not require the stoichiometry to alter to that given by (3‴) under normal conditions of synthesis. Unlike the defect equilibria theory of Smyth et al. [29] which implies a continuous change in cation stoichiometry to accompany a change in oxygen content, we regard the two mechanisms (1–1‴) and (4, 4′) as two entirely separate mechanisms which can occur either independently or together. Thus, samples fired at 1400°C in O_2 have equilibria and formulae given by (1–1‴); on firing in

air at 1400°C of either unreacted samples or samples previously fired in O_2, a small amount of O_2 loss given by (4, 4′) occurs.

We find no evidence of (2–2‴) nor of (3–3‴) in bulk samples heated in air or argon. It is highly likely, however, that under strongly reducing conditions, mechanism (3–3‴) may occur. Recently Makovec et al. [40] prepared single phase electronically compensated materials $Ba_{1-z}La_zTiO_3$, with $0 \leq z \leq 0.10$, under suitably reducing conditions (10%H_2/90%N_2 atmosphere at temperatures 1150–1350°C). On reoxidation in air, at temperatures 1150–1350°C, the materials tended to Ti vacancy compensation (1–1‴) with concomitant precipitation of $Ba_6Ti_{17}O_{40}$ to allow the change in cation stoichiometry. It would be interesting to establish precisely the conditions under which (3–3‴) could be obtained, and to compare them with those needed to observe (4, 4′).

A proper study of defect equilibria in doped $BaTiO_3$ requires a careful separation of thermodynamic and kinetic factors. The differences in electrical properties found here on firing in different atmospheres at 1400°C illustrates the importance of both of these: the equilibrium defect structure at e.g. 1400°C is very sensitive to atmosphere and therefore, on changing the temperature or atmosphere (e.g. by cooling samples for subsequent property measurements at lower temperature), great care is required to ensure either that no change in defect structure/composition occurs or that sufficient time is allowed for a new equilibrium state to be reached. In practice, it is likely that non-equilibrium structures may result, such as in samples with oxidized surfaces and reduced cores and it is important to recognize these in order to adequately analyse and interpret data. Nowotny and Rekus [41] studied the equilibration kinetics of Nb-doped $BaTiO_3$ ceramics by measuring conductivity as a function of temperature and oxygen partial pressure. They demonstrated that long equilibration times are often required to obtain equilibrium conductivity values. For example, on cooling a 0.05 atom% Nb-doped ceramic from 1035 to 943°C at $P_{O_2} = 220$ Pa, an equilibration time in excess of 4 months was required. They highlighted the necessity to differentiate between "equilibrium" and "stationary" states when varying temperature and/or P_{O_2} and suggested that the lack of conductivity dependence on P_{O_2} observed by Chan and Smyth [2, 3] for La-doped $BaTiO_3$ ceramics indicates that their electrical conductivity data do not correspond to equilibrium values.

Unresolved questions over the semiconductivity of doped $BaTiO_3$ induced by loss of oxygen from the crystal lattice are (a) is the degree of oxygen loss under equilibrium conditions variable to a significant degree with (i) temperature and (ii) La content, (b) is the oxygen loss under equilibrium conditions uniform throughout the sample or is it preferentially associated with grain boundaries and surfaces, (c) what are the relative contributions of (i) kinetic and (ii) thermodynamic factors to the extent of reaction (3) under varying experimental conditions and (d) what is the role of ceramic microstructure on both the extent of oxygen loss and the kinetics of oxygen loss/uptake? Determination of oxygen diffusion rates, particularly as a function of $[V_O^{\bullet\bullet}]$, in undoped and La-doped $BaTiO_3$ is also required. To date, much of the data are assumed from chemical diffusivity data determined from equilibrium conductivity measurements, with no consideration given to the role of oxygen vacancies [2–4, 42]. These data, and oxygen diffusion data obtained from other methods have largely been collected from multiphase compositions and show significant discrepancies, with both an increase [31] and a decrease [4] in oxygen diffusion rate claimed on La-doping.

Conclusions

The La-doping mechanism in $BaTiO_3$ ceramics heated in air or oxygen at ca. 1350°C solely involves direct substitution of La for Ba with concomitant creation of Ti vacancies to maintain charge balance. No evidence for compensation by either electronic or Ba vacancy mechanisms was observed under these conditions. Superposed on this ionic compensation mechanism, oxygen loss occurs for samples heated at high temperature ($\geq$1350°C) in air, which gives rise to electronic compensation and n-type semiconductivity. This appears to be an independent mechanism since it occurs in samples prepared with Ti vacancies as the main compensation mechanism and does not involve any precipitation or changes to the cationic composition of the solid solutions. Thus, we suggest that oxygen loss from the lattice is responsible for semiconductivity in La-doped materials heated in air and that the widely-held view that direct donor-doping by La is responsible for the semiconductivity is not correct.

A switch in mechanism from Ti vacancy to electronic compensation on reducing P_{O_2} would require a change in cation stoichiometry. No evidence of

secondary phases was observed by TEM for any sample prepared in air or argon according to the Ti-vacancy mechanism, where $x < 0.25$, irrespective of whether the sample was electrically insulating or semiconducting at room temperature. Thus, we see no need to include a precipitation reaction; instead, the results are qualitatively consistent with a simple defect model for binary oxides [43].

Whilst our initial studies focused on compositions that lay on the hypothetical, electronic compensation join, $Ba_{1-z}La_zTiO_3$ and that appeared always to be multiphase when heated in air, subsequent studies on the Ti vacancy join showed that single phase solid solutions could be made semiconducting by varying the atmosphere during heating.

Acknowledgments

We thank EPSRC for support (FDM) and Dr E.E. Lachowski (Department of Chemistry, University of Aberdeen) for TEM analysis and advice on SEM technique.

Note

1. There is some semantic confusion over use of the terms 'donor' and 'acceptor' dopant. Some authors reserve these terms for dopants that lead to a change in electrical properties by creating electrons and holes, respectively. Others adopt a wider meaning in which a donor (acceptor) dopant has higher (lower) charge than the ion that it replaces; a charge compensation mechanism is then required for such aliovalent substitution and this may be either electronic or ionic. Usually the intended meaning of these terms is clear, but not always.

References

1. J. Nowotny and M. Rekas, *Solid State Ionics*, **49**, 135 (1991).
2. N.-H. Chan and D. M. Smyth, *J. Electrochem. Soc.*, **123**(10), 1584 (1976).
3. N.-H. Chan and D. M. Smyth, *J. Am. Ceram. Soc.*, **67**(4), 285 (1984).
4. J. Daniels, K.H. Hardtl, D. Hennings, and R. Wernicke, *Philips Res. Repts.*, **31**, 487 (1976).
5. G.H. Jonker and E.E. Havinga, *Mat. Res. Bull.*, **17**, 345 (1982).
6. D. Makovec, Z. Samardzija, U. Delalut, and D. Kolar, *J. Am. Ceram. Soc.*, **78**(8), 2193 (1995).
7. F.D. Morrison, D.C. Sinclair, J.M.S. Skakle, and A.R. West, *J. Am. Ceram. Soc.*, **81**(7), 1957 (1998).
8. S. Škapin, D. Kolar, D. Suvorov, and Z. Samardzija, *J. Mater. Res.*, **13**(5), 1327 (1998).
9. G.V. Lewis and C.R.A. Catlow, *J. Phys. Chem. Solids*, **47**(1), 89 (1986).
10. O. Saburi, *J. Phys. Soc. Jpn.*, **14**(9), 1159 (1959).
11. V.J. Tennery and R.L. Cook, *J. Am. Ceram. Soc.*, **44**(4), 187 (1961).
12. S.B. Desu, *Ceramic Transactions*, **8**, 157 (1990).
13. C.-J. Peng and H.-Y. Lu, *J. Am. Ceram. Soc.*, **71**(44), C-44 (1988).
14. T.-B. Wu and J.-N. Lin, *J. Am. Ceram. Soc.*, **77**(3), 759 (1994).
15. A.B. Alles, V.R.W. Amarakoon, and V.L. Burdick, *J. Am. Ceram. Soc.*, **72**(1), 148 (1989).
16. F.D. Morrison, D.C. Sinclair, and A.R. West, *J. Am. Ceram. Soc.*, **84**(3), 531 (2001).
17. P.G. Bruce and A.R. West, *J. Electrochem. Soc.*, **130**, 662 (1983).
18. D.E. Johnston, Ph.D. Thesis, University of Aberdeen (1993).
19. Scribner Associates, Inc. Charlottesville, Virginia.
20. N. Hirose and A.R. West, *J. Am. Ceram. Soc.*, **79**(6), 1633 (1996).
21. J.T.S. Irvine, D.C. Sinclair, and A.R. West, *Adv. Mater.*, **2**(3), 132 (1990).
22. D.C. Sinclair and A.R. West, *J. Appl. Phys.*, **66**(8), 3850 (1989).
23. Joint Committee for Powder Diffraction Standards, card no. 35-815.
24. F.D. Morrison, D.C. Sinclair, and A.R. West, *J. Appl. Phys.*, **86**(11), 6355 (1999).
25. G.H. Jonker, *Solid State Electron.*, **7**, 895 (1964).
26. G. Goodman, *J. Am. Ceram. Soc.*, **46**(1), 48 (1963).
27. W. Hewang, *J. Am. Ceram. Soc.*, **47**(10), 484 (1964).
28. W. Hewang, *J. Mat. Sci.*, **6**, 1214 (1971).
29. H.M. Chan, M.P. Harmer, and D.M. Smyth, *J. Am. Ceram. Soc.*, **69**(6), 507 (1986).
30. R.J. Borg and G.J. Dienes, *An Introduction to Solid State Diffusion* (Academic Press, London, 1988).
31. S. Shirasaki, H. Yamamura, H. Haneda, K. Kakegawa, and J. Moori, *J. Chem. Phys.*, **73**(9), 4640 (1980).
32. H. Sasaki and Y. Matsuo, *J. Am. Ceram. Soc.*, **48**(8), 434 (1965).
33. J. Maier, J. Jamnik, and M. Leonhardt, *Solid State Ionics*, **129**, 25 (2000).
34. I. Denk, F. Noll, and J. Maier, *J. Am. Ceram. Soc.*, **80**(2), 279 (1997).
35. I. Denk, W. Münch, and J. Maier, *J. Am. Ceram. Soc.*, **78**(12), 3265 (1995).
36. J.B. MacChesney and J.F. Potter, *J. Am. Ceram. Soc.*, **48**(2), 81 (1965).
37. M. Kuwabara and H. Matsuda, *J. Am. Ceram. Soc.*, **80**(10), 2590 (1997).
38. S. Shirasaki, H. Haneda, K. Arai, and M. Fujimoto, *J. Mat. Sci.*, **22**, 4439 (1987).
39. J.B. MacChesney, P.K. Gallagher, and F.V. DiMarcello, *J. Am. Ceram. Soc.*, **46**(5), 197 (1963).
40. D. Makovec and M. Drofenik, *J. Am. Ceram. Soc.*, **83**(10), 2593 (2000).
41. J. Nowotny and M. Rekas, *Ceramics International*, **20**, 265 (1994).
42. (a) C.R. Song and H.-I. Yoo, *Solid State Ionics*, **120**, 141 (1999). (b) C.R. Song and H.-I. Yoo, *Phys. Rev. B.*, **61**(6), 3975 (2000). (c) C.R. Song and H.-I. Yoo, *Solid State Ionics*, **124**, 289 (1999). (d) C.R. Song and H.-I. Yoo, *J. Am. Ceram. Soc.*, **83**(4), 773 (2000).
43. D.M. Smyth, *Solid State Ionics*, **129**, 5 (2000).